2017

Diffusion-steered denoising framework for suppressing multiplicative noise in ultrasonogra

Michael, Kisangiri

African Journal of Applied Research

2408-7920

African Journal of Applied Research
Vol. 3, No. 2 (2017), pp. 58-72
http://www.ajaronline.com
http://doi.org/10.26437/ajar.03.02.2017.05

DIFFUSION-STEERED DENOISING FRAMEWORK FOR SUPPRESSING MULTIPLICATIVE NOISE IN ULTRASONOGRAMS

[1]Kessy, S. J., [2]Msuya, H. G., [3]Kisangiri, M., and [4]Maiseli, B. J.
[1&3]Department of Communication Science & Engineering, Nelson Mandela African Institute of Science & Technology, Tanzania
[2&4]Department of Electronics & Telecommunication Engineering, University of Dar es Salaam, Tanzania.

Abstract

Ultrasound imaging, a non-invasive and cost-effective imaging modality, is probably the most preferred diagnostic tool in medicine. Despite its merits, ultrasonograms are usually corrupted by multiplicative noise, a consequence that limits doctors to provide more accurate treatments and decisions. Attempts to address the problem have been made, but we have found little works that adopt the diffusion framework, which scholars have reported that it produces promising results in additive noise cases. In the current work, we have modified the classical Perona-Malik (PM) diffusion model to deal with multiplicative noise. Inspired by the ability of PM to restore semantically critical features, we have embedded a log-based regularization term, statistically modeled to mitigate multiplicative effects in the ultrasound images, into the modified PM. Additionally, the diffusivity kernel of PM has been re-designed to ensure that the diffusion process is properly steered. Modification of the PM kernel was achieved through integration of the half-quadratic diffusivity, which has a corresponding energy functional that is strictly convex, a promising mathematical property that encourages unique solutions and guarantees stability of the evolutionary system. Our interest is to emphasize regularization in flat image regions while maintaining plausible edges and contours. Subjective and quantitative evaluations demonstrate that the proposed model produces better results compared with some state-of-the-art methods. Even more importantly, our approach guarantees convergence, stability, and robustness when tested for a range of ultrasonograms. Probably the intriguing property of our framework is its ability to evolve a denoising image over a longer period without smudging or destroying its sensitive features. The proposed approach may further be extended and actualized in practical imaging devices.

Keywords: *Denoising, anisotropic diffusion, ultrasound image, optimization, Perona-Malik.*

ISSN: 2408-7920

African Journal of Applied Research
Vol. 3, No. 2 (2017), pp. 58-72
http://www.ajaronline.com
http://doi.org/10.26437/ajar.03.02.2017.05

INTRODUCTION

Ultrasonography refers to a diagnostic medical procedure that employs sound waves to visualize internal structures of the body. Images generated through this technique are called ultrasonograms, and are often cast in screens constructed by special materials. Ultrasonography (also called ultrasound imaging), is widely applied to diagnose tissues and organs in humans, It is non-invasive, portable, cost-effective, real-time driven, and practically harmless. The technique can produce audible sounds of blood flow to collect measures suitable for biomarkers in diagnosis (Loizou et al., 2005). Because of these merits, ultrasound imaging is probably one of the most prevalent diagnostic techniques preferred by people for treatments.

Despite the potential values of ultrasound imaging, ultrasonograms (particularly the B-mode types) usually suffer from speckle or multiplicative noises. Since 1970s, scholars have been reporting the impacts of multiplicative noise in ultrasonograms: in (Dutt, 1995), the author employed statistical approaches to model speckle noise as a complex random motion, represented as a sum of a larger number of complex phasors that occur when at least two waves scattered from different regions of the organ under investigation interfere constructively or destructively, a phenomenon that forms bright and dark spots on the image. In practical applications, these undesirable consequences lower the usefulness of the image in subsequent sub-domain tasks: registration, segmentation, feature extraction, analysis and recognition, and reconstruction. Also, multiplicative noise complicates quantitative measurements (Aysal & Barner, 2007), an effect that makes the images less useful in machine-driven tasks. Therefore, suppressing noise in ultrasonograms is essentially important for proper clinical interpretation and quantitative measurements.

Numerous methods have been developed to improve quality of the ultrasound images. In (Mahmoud, Rabaie, Taha, Zahran, & El-samie, 2013),the authors compared different denoising filters, designed in both spatial and frequency domains, for reducing speckle noise. Other methods for removing noise are based on total variation (Afonso & Sanches, 2015; Dong et al., 2017; Hacini, Hachouf, & Djemal, 2014; Liu, Huang, Xu, & Lv, 2013; Lv, Le, Huang, & Jun, 2013; Rudin, Osher, & Fatemi, 1992; Shama, Huang, Liu, & Wang, 2016; Wu & Feng, 2015), wavelet (Chang, Yu, & Vetterli, 2000; Donoho & Johnstone, 1994; Kour & Kaur, 2016; Mastriani, 2008; Zhang, Lin, Wu, Wang, & Cheng, 2015), and linear/nonlinear diffusion (Bhateja, Singh, Srivastava, & Singh, 2014; Hu & Tang, 2016; Perona & Malik, 1990; Ramos-Llordén, Vegas-Sánchez-Ferrero, Martin-Fernandez, Alberola-López, & Aja-Fernández, 2015; Xu, Jia, Shi, & Pang, 2016). Of the classes of noise-suppressing methods, the ones based on nonlinear diffusion have gained considerable attention of scholars for their ability to remove noise while protecting critical image features (Liu & Liu, 2012; Maleki, Narayan, & Baraniuk, 2013; Weickert & Benhamouda, 1997). In (Perona & Malik, 1990), Perona and Malik established a nonlinear diffusion model that integrates a feature-dependent kernel that steers the smoothing process in the discriminatory fashion: flat regions and edges in the image receive stronger and

ISSN: 2408-7920

African Journal of Applied Research
Vol. 3, No. 2 (2017), pp. 58-72
http://www.ajaronline.com
http://doi.org/10.26437/ajar.03.02.2017.05

weaker smoothing respectively, an intelligible technique that restores high quality images. The Perona-Malik model, however, suffers from staircasing problems and tends to add speckles into the evolving solutions (Guo, Sun, Zhang, & Wu, 2012; Wu, Ogada, Sun, & Guo, 2014). Furthermore, the corresponding energy functional of the model is non-convex, a property that may cause the model to generate multiple solutions.

Scholars have attempted to address weaknesses of the Perona-Malik (PM) model (Attivissimo, Cavone, Lanzolla, & Spadavecchia, 2010; Kour & Kaur, 2016; Kumar & Rattan, 2012; Liu & Liu, 2012; Maiseli, 2016; Maiseli & Gao, 2016; Noe, Workshop, & Palmas, 2006; Xu et al., 2016) But, most of the improvements concentrate on removing additive noise. In the current work, we have integrated a prior term, statistically modeled to eliminate multiplicative noise, into the modified version of the Perona-Malik framework. Additionally, the non-convex nature of PM potential has been addressed using the half-quadratic technique proposed by Charbonnier et al. (Charbonnier, Blanc-Feraud, Aubert, & Barlaud, 1994) .

PROPOSED DIFFUSION-DRIVEN MODEL

Motivated by the limitations of the original Perona-Malik model, we propose the minimization problem

$$\min_u \left\{ \int_\Omega K^2 \left(\sqrt{1 + \left(\frac{|\nabla u|}{K} \right)^2} - 1 \right) dx + \lambda \int_\Omega \left(\log u + \frac{f}{u} \right) dx \right\}, \qquad (1)$$

where the first and second parts of the formulation's integrands represent the energy functional, $\rho(s = |\nabla u|)$, and the fidelity term, respectively; K is the shape-defining constant; u is the denoising (ideal) image; f is the noisy image corrupted by multiplicative noise; λ is the regularization term; and Ω is the supporting domain of u or f.

Proof: To prove that our energy functional is convex, we should perform the second derivative test on ρ. Therefore,

$$\rho''(s) = \frac{1}{\left(1 + \left(\frac{s}{K}\right)^2\right)^{\frac{3}{2}}} > 0. \qquad (2)$$

The positivity of ρ'' implies that ρ is strictly a convex energy functional, a mathematical property that signals stability and uniqueness of the evolving solution.

Applying the Euler-Lagrange equation to (1) and subjecting the resulting formulation into a dynamical system, we get

ISSN: 2408-7920

African Journal of Applied Research
Vol. 3, No. 2 (2017), pp. 58-72
http://www.ajaronline.com
http://doi.org/10.26437/ajar.03.02.2017.05

$$\frac{\partial u}{\partial t} = \nabla \cdot \left(\frac{1}{\sqrt{1 + \left(\frac{|\nabla u|}{K}\right)^2}} \nabla u \right) - \lambda \left(\frac{u - f}{u^2} \right),$$

$$(x, t) \in \Omega \times (0, T) \tag{3}$$

$$u(x, 0) = f, x \in \Omega \tag{4}$$

$$\frac{\partial u}{\partial \vec{n}} = 0, (x, t) \in \partial\Omega \times (0, T), \tag{5}$$

Where Ω is the supporting domain of u and T represents the total evolution time. To understand how (3) reacts against edges, the equation should be decomposed into tangential, u_{TT}, and normal, u_{NN}, components along the isophotes lines of u (Figure 1). Thus, let $u(x, y)$ be the intensity of u at the position (x, y), where $|\nabla u(x, y)| \neq 0$. Furthermore, let $T(x) = (u_x, u_y)/|\nabla u|$ and $N(x) = (-u_y, u_x)/|\nabla u|$ be orthogonal vectors, where u_x and u_y are the first-order partial derivatives of u. Also, let u_{TT} and u_{NN} be the second-order partial derivatives of u along T and N directions, respectively, and given as

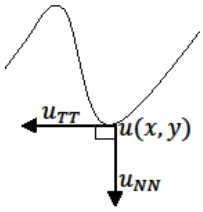

Figure 1. Tangential (u_{TT}) and normal (u_{NN}) components along the isophote lines.

$$u_{TT} = T' \nabla^2 u T = \frac{1}{|\nabla u|^2} \left(u_x^2 u_{yy} + u_y^2 u_{xx} - 2 u_x u_y u_{xy} \right) \tag{6}$$

and

$$u_{NN} = N' \nabla^2 u N = \frac{1}{|\nabla u|^2} \left(u_x^2 u_{xx} + u_y^2 u_{yy} + 2 u_x u_y u_{xy} \right), \tag{7}$$

Where $\nabla^2 u$ represents the Hessian matrix of u. Then, the decomposed formulation of (3) can be represented as

$$\frac{\partial u}{\partial t} = \frac{\rho'(|\nabla u|)}{|\nabla u|} u_{TT} + \rho''(|\nabla u|) u_{NN} - \lambda \left(\frac{u - f}{u^2} \right). \tag{8}$$

Simplifying (8) gives

ISSN: 2408-7920

African Journal of Applied Research
Vol. 3, No. 2 (2017), pp. 58-72
http://www.ajaronline.com
http://doi.org/10.26437/ajar.03.02.2017.05

$$\frac{\partial u}{\partial t} = \frac{1}{\sqrt{1+\left(\frac{|\nabla u|}{K}\right)^2}} u_{TT} + \frac{1}{\left(\sqrt{1+\left(\frac{|\nabla u|}{K}\right)^2}\right)^3} u_{NN} - \lambda\left(\frac{u-f}{u^2}\right). \quad (9)$$

The formulation in (9) provides some useful edge-preserving characteristics: first, the model encourages forward diffusion, a property that ensures regularity in the smoothing process. Second, u_{TT} and u_{NN} are properly balanced to promote the edge-driven regularization behavior. In smooth image regions where$|\nabla u| \to 0$, (9) reduces to

$$\frac{\partial u}{\partial t} = u_{TT} + u_{NN} - \lambda\left(\frac{u-f}{u^2}\right), \quad (10)$$

This implies that these regions receive uniform smoothing similar to the heat equation. Near edges where $|\nabla u| \to \infty$, the coefficient of u_{NN}, which has a larger denominator, diminishes faster than that of u_{TT}. This dominance behavior of the u_{TT} component causes the proposed model to preserve meaningful image features.

Numerical implementation

Our framework was implemented using the four-point explicit numerical scheme, which computes dependent variables using the known values. This type of scheme is simple and generates convincing results that are more accurate and reliable (Langtangen, 2013). Let ∇_W,∇_N, ∇_S, and ∇_E represent image gradients in the West, North, South, and East directions in the scheme. Then, the discrete image gradients can be defined as

$$\nabla_W u_{i,j} = u_{i,j-1} - u_{i,j}, \ \nabla_N u_{i,j} = u_{i-1,j} - u_{i,j},$$

$$\nabla_S u_{i,j} = u_{i+1,j} - u_{i,j}, \text{ and } \nabla_E u_{i,j} = u_{i,j+1} - u_{i,j}$$

for $0 \le i \le I$ (number of rows) and $0 \le j \le J$ (number of columns). The corresponding discrete conduction coefficients are

$$C_W = \frac{1}{\sqrt{1+\left(\frac{|\nabla_W u_{i,j}|}{K}\right)^2}}, \ C_N = \frac{1}{\sqrt{1+\left(\frac{|\nabla_N u_{i,j}|}{K}\right)^2}},$$

$$C_S = \frac{1}{\sqrt{1+\left(\frac{|\nabla_S u_{i,j}|}{K}\right)^2}}, \text{ and } C_E = \frac{1}{\sqrt{1+\left(\frac{|\nabla_E u_{i,j}|}{K}\right)^2}}.$$

ISSN: 2408-7920

African Journal of Applied Research
Vol. 3, No. 2 (2017), pp. 58-72
http://www.ajaronline.com
http://doi.org/10.26437/ajar.03.02.2017.05

Therefore, the discretized divergence term can be defined as

$$\mathrm{div}_{i,j} = C_N \nabla_N u_{i,j} + C_S \nabla_S u_{i,j} + C_W \nabla_W u_{i,j} + C_E \nabla_E u_{i,j} \quad (11)$$

and the steepest descent equation is

$$u_{i,j}^{n+1} = u_{i,j}^{n} + \tau(\mathrm{div}_{i,j}^{n} - \lambda(u_{i,j}^{n} - f_{i,j}^{n})/((u_{i,j}^{n})^2 + \epsilon)), \quad (12)$$

where $u_{i,j}^{0} = f_{i,j} = f(ih, jh)$, $u_{i,0}^{n} = u_{i,1}^{n}$, $u_{0,j}^{n} = u_{1,j}^{n}$, $u_{I,i}^{n} = u_{I-1,i}^{n}$, and $u_{i,J}^{n} = u_{i,J-1}^{n}$; h is the grid step size and $\epsilon > 0$ defines a small stabilizing constant.

EXPERIMENTS

Several experiments were conducted to test the performances of various denoising methods: PM (Perona & Malik, 1990), Total variation (Rudin et al., 1992), Guo (Guo et al., 2012) and Charbonnier (Charbonnier et al., 1994). In the first experiment, speckle (multiplicative) noise of density 0.04 was added into two different synthetic images, each 300×300 in size, namely "Geometry" and "Squares". Next, the methods were applied on the noisy images to recover their original versions. Then, objective quality metrics, namely PSNR (peak signal to noise ratio) and SSIM (structural similarity) were used to evaluate the restoration results for each method. The aspect of edge recovery was tested through image profiles: for each restored image, a line graph through intensity values along a specific row (arbitrarily taken half way on the vertical dimension) was drawn. These profiles were compared against those of the original and noisy images. We also executed an experiment to compare stability aspects between our model and that proposed by Perona and Malik. In this case, the noisy synthetic images were evolved by the models over 1000, 3000, and 5000 iterations. We define a stable method as the one that can maintain a peak quality value (PSNR or SSIM) regardless of the number of iterations. In fact, this observation is the expected attribute for a convex energy functional like ours.

ISSN: 2408-7920

African Journal of Applied Research
Vol. 3, No. 2 (2017), pp. 58-72
http://www.ajaronline.com
http://doi.org/10.26437/ajar.03.02.2017.05

The second experiment involved real images of common carotid arteries (CCAs) corrupted by multiplicative noises. These CCAs were imaged from different patients. Then, the noise removal methods were applied to the images in an attempt to restore their (unknown) original versions. Because of a lack of the ground-truth images, comparisons on the results generated from various methods were done subjectively through visual assessments: an appealing image contains more details and holds semantically important features (edges, contours, and lines). In all experiments, parameters of the proposed model were fixed: $K = 0.09$, $\lambda = 2.90$, $dt = 0.07$, and $\epsilon = 1 \times 10^{-6}$. Simulations were conducted using MATLAB R2016b. Implementation codes of our framework have been shared in the MatlabCentral[1] public repository.

Performance Evaluation

To quantify the quality of our model, we used PSNR (Wang & Bovik, 2009) and SSIM (Wang, Bovik, Sheikh, & Simoncelli, 2004) performance indices. PSNR measures signal strength in the image with respect to noise, and is governed by the equation

$$\text{PSNR} = 20\log_{10}\left(\frac{MAX_f}{\sqrt{MSE}}\right), \tag{13}$$

where MAX_f is the maximum gray level in f and MSE represents the mean squared error. Higher value of PSNR signifies a stronger signal and vice versa. Scholars have, however, criticized the metric because it fails to emulate the human visual system(Wang et al., 2004) . Hence, SSIM was proposed to address the challenge. This quality index is defined as

$$\text{SSIM} = \frac{(2\mu_u\mu_f + C_1)(2\sigma_{uf} + C_2)}{(\mu_u^2 + \mu_f^2 + C_1)(\sigma_u^2 + \sigma_f^2 + C_2)}, \tag{14}$$

[1]https://www.mathworks.com/matlabcentral/fileexchange/62569-diffusion-steered-denoising-framework-for-suppressing-multiplicative-noise-in-ultrasonograms

ISSN: 2408-7920

African Journal of Applied Research
Vol. 3, No. 2 (2017), pp. 58-72
http://www.ajaronline.com
http://doi.org/10.26437/ajar.03.02.2017.05

where, μ_u and μ_f are the averages of u and f, respectively; σ_{uf} is the covariance of u and f; σ_u and σ_f are the standard deviations of u and f, respectively; and C_1 and C_2 are the stabilizing constants. The value of SSIM ranges between 0 and 1. SSIM is higher for a visually appealing image, and vice versa.

RESULTS AND DISCUSSION

Quantitative results demonstrate that the proposed method maintains the peak quality values over a longer period (Figure 2). This observation indicates that our framework guarantees stability and may be applied with little restrictions on the number of iterations. (Figure 3) shows that, even at larger iteration numbers, our framework generates appealing images containing useful features. The framework's stability is attributed to the convexity of our energy functional, a property that reinforces convergence of the evolution system. On the contrary, the Perona-Malik model tends to smudge and blur critical image features as the evolution system advances. Investigating profile maps, the proposed method shows that it generates sharper curves that are closer to the original ones (Figure 4). Hence, we infer that our approach can produce plausible edges. Numerical results in Table 1 further insist higher PSNR and MSSIM values attained by our method.

Visual results from synthetic images demonstrate that the proposed method suppresses noise more effectively and restores images with lower errors (Figures 5). Furthermore, compared with other denoising methods, our approach generates promising restoration results when applied to CCA images (Figures 6). Coupled with several strengths, the observation justifies our claims that the proposed noise-suppressing framework may be suitable to denoise ultrasound images corrupted by natural noise. From (Figures 6), the restored CCA images by our method are detailed and lack unnecessary artifacts, the observation that can assist doctors to provide more accurate and appropriate treatments to patients.

Appealing visual and subjective results demonstrated by our framework can be explained in the perspective of the decomposed formulation in (9), which shows an effective interplay between u_{TT} and u_{NN} regularization components. The equation gives an idea that the proposed denoising method describes forward diffusion that strengthen edges and contours, as depicted through the denoising results of synthetic images. Presence of the backward diffusion, however, would further enhance our results because this mode of noise removal tends to sharpen critical image features. Perhaps one approach to achieve both forward and backward diffusions is to integrate other types of smoothing functionals, such as the total variation, into the current framework. The integration should be done in such a way that potential characteristics of these other functionals are harnessed properly. It may be interesting, for instance, to investigate how the Charbonnier model, which has been adopted in the current study, and the TV model can be integrated into the

African Journal of Applied Research
Vol. 3, No. 2 (2017), pp. 58-72
http://www.ajaronline.com
http://doi.org/10.26437/ajar.03.02.2017.05

denoising framework to produce optimal results, sharper and detailed images with superior objective quality values.

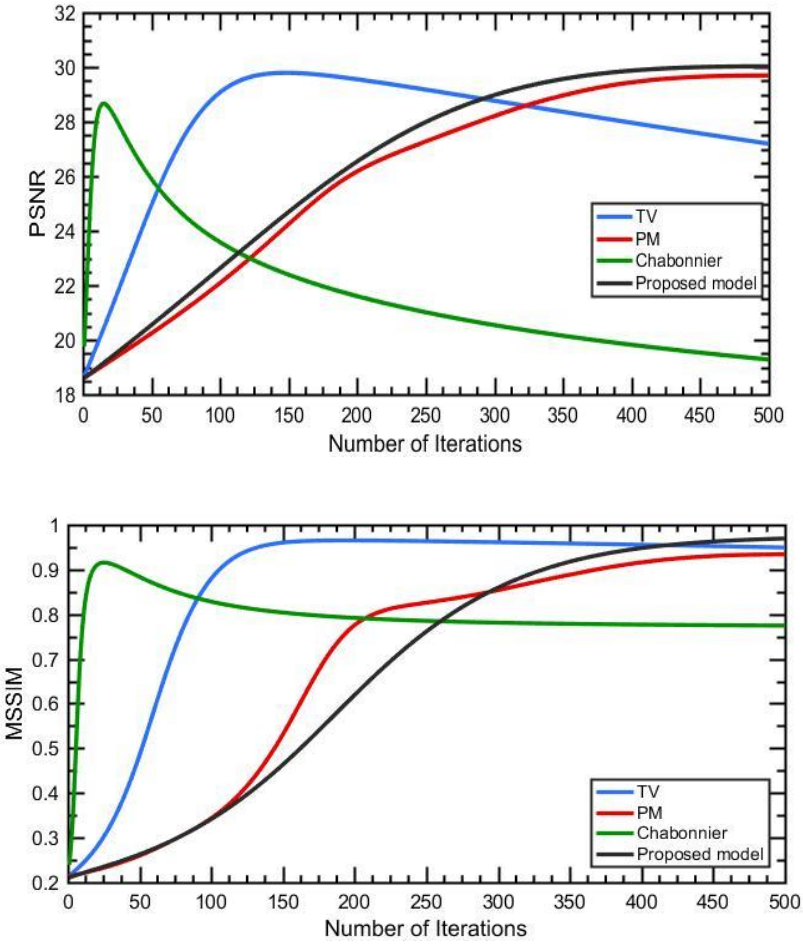

Figure 2: Peak-signal-to-noise-ratio (PSNR) and structural similarity (SSIM) versus number of iterations.

ISSN: 2408-7920

African Journal of Applied Research
Vol. 3, No. 2 (2017), pp. 58-72
http://www.ajaronline.com
http://doi.org/10.26437/ajar.03.02.2017.05

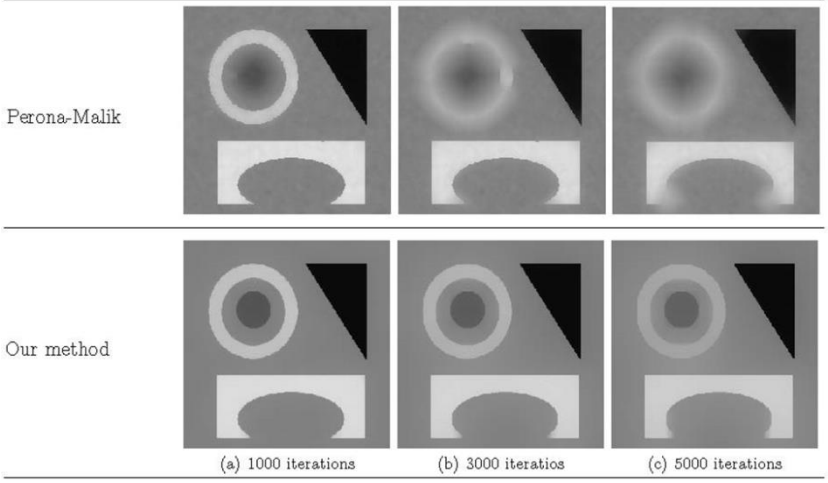

Figure 3: Perona-Malik model and our method applied on the noisy "Geometry" synthetic image. Experiments executed for different number of iterations.

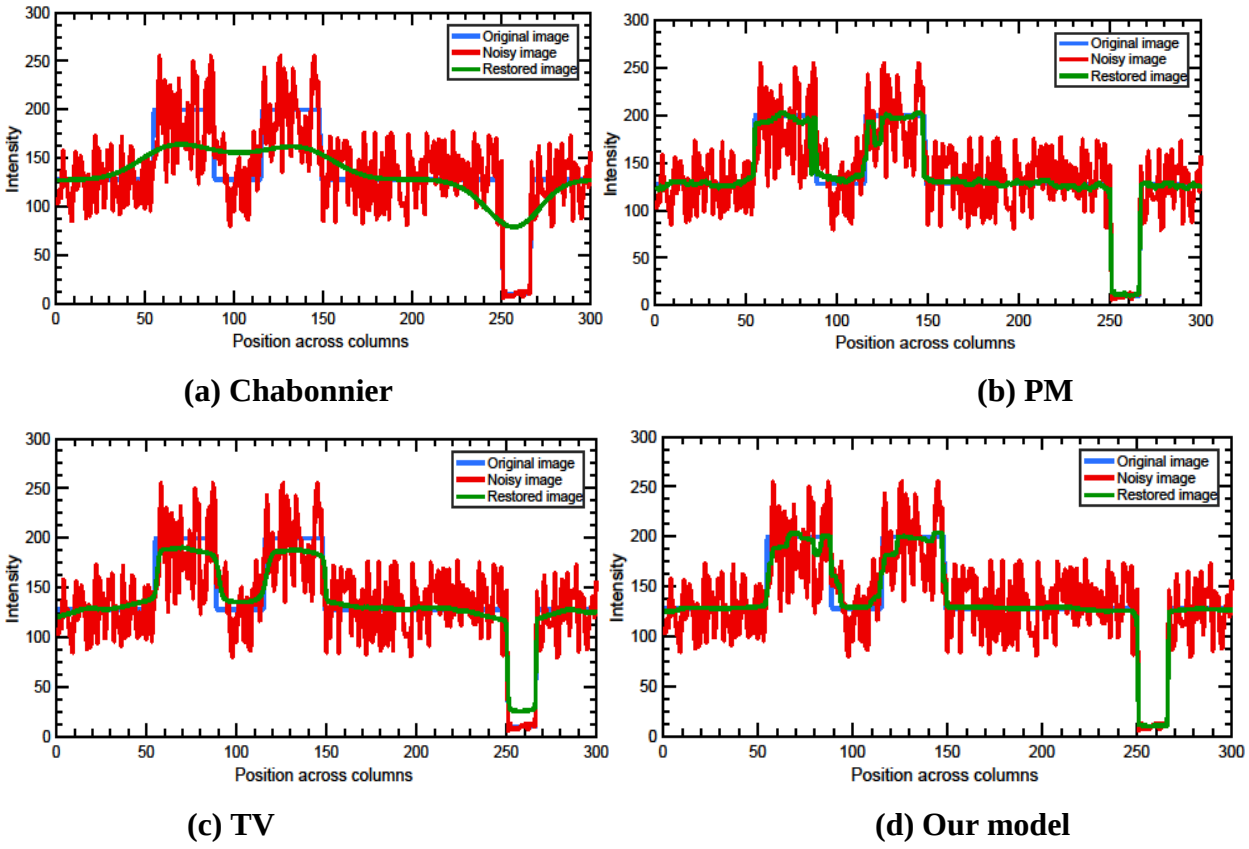

Figure 4: Intensity image profiles of different denoising methods.

ISSN: 2408-7920

African Journal of Applied Research
Vol. 3, No. 2 (2017), pp. 58-72
http://www.ajaronline.com
http://doi.org/10.26437/ajar.03.02.2017.05

Table 1: PSNR (peak-signal-to-noise-ratio) and SSIM (structural similarity) of images generated by different methods.

Method	PSNR		SSIM	
	Geometry	Squares	Geometry	Squares
Guo	25.55	25.25	0.8684	0.9183
PM	29.09	30.22	0.9175	0.9221
Charbonnier	29.59	29.90	0.9254	0.9508
TV	30.87	30.49	0.9523	0.9851
Proposed model	**31.11**	**30.65**	**0.9770**	**0.9917**

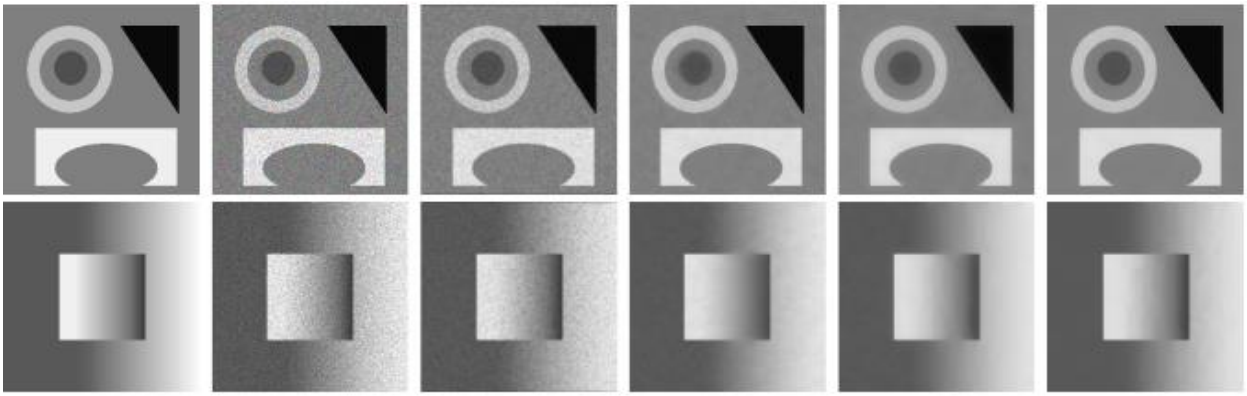

(a) Original (b) Noisy (c) Guo (d) PM (e) TV (f) Ours

Figure 5: Different denoising methods applied on the noisy synthetic images: first row, denoising results of "Geometry"; and second row, "Squares" synthetic images. PM (Perona-Malik) and TV (Total Variation).

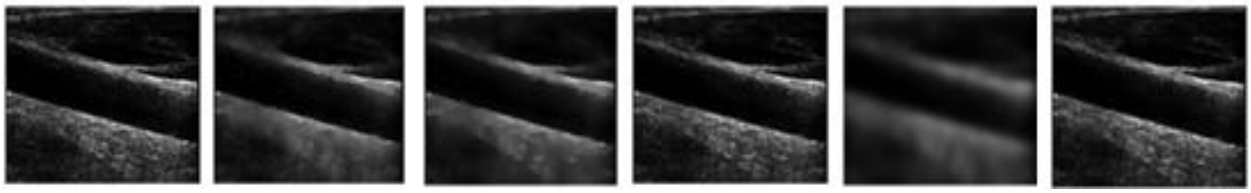

ISSN: 2408-7920

African Journal of Applied Research
Vol. 3, No. 2 (2017), pp. 58-72
http://www.ajaronline.com
http://doi.org/10.26437/ajar.03.02.2017.05

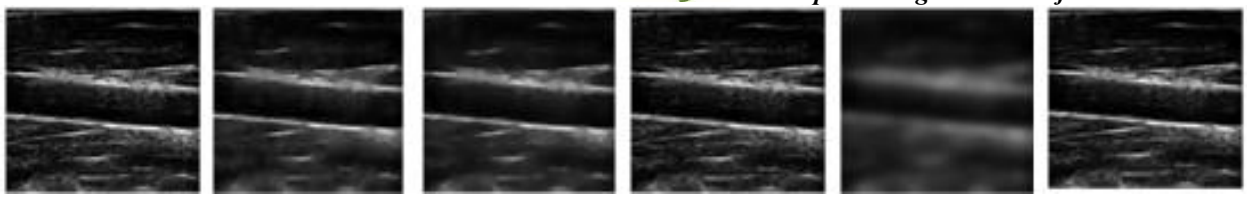

(a) Noisy (b) PM (c) TV (d) Guo (e) Charb (f) Ours

Figure 6: Different denoising methods applied on a noisy common carotid artery: first row, patient #1 and second row, patient #2.

CONCLUSION

We have proposed a diffusion-steered framework to suppress noise in ultrasound images. Our method incorporates a strictly convex Charbonnier potential and a prior term adapted for multiplicative noise types. The corresponding energy functional of the proposed model offers promising mathematical properties (smoothness, convexity, and stability) that ensure favorable solutions. Experimental results demonstrate that the proposed approach generates appealing images that contain higher values of PSNR and SSIM compared with other classical methods. We have applied the new method on actual ultrasonograms to demonstrate the effectiveness of our framework in real-world applications.

Acknowledgment

This work was supported by DAAD (Deutscher Akademischer Austauschdienst) organization under the grant numbers 57191505 and 57349843. Also, we would like to give our sincere gratitude to Prof. Gitta Domik (PhD) for her invaluable comments and suggestions to improve the quality of our work. Equally important, we thank the University of Paderborn, particularly the Computer Graphics, Visualization, and Image Processing research group, and the Nelson Mandela African Institute of Science and Technology for their social and academic support that positively impacted our study

Competing interests

The authors declare that they have no competing interests to disclose.

REFERENCES

Afonso, M., & Sanches, J. M. (2015). Image reconstruction under multiplicative speckle noise using total variation. *Neurocomputing*, *150*(Part A), 200–213. http://doi.org/10.1016/j.neucom.2014.08.073

Attivissimo, F., Cavone, G., Lanzolla, A. M. L., & Spadavecchia, M. (2010). A technique to improve the image quality in computer tomography. *IEEE Transactions on Instrumentation and Measurement*, *59*(5), 1251–1257. http://doi.org/10.1109/TIM.2010.2040932

ISSN: 2408-7920

Aysal, T. C., & Barner, K. E. (2007). Rayleigh-maximum-likelihood filtering for speckle reduction of ultrasound images. *IEEE Transactions on Medical Imaging*, *26*(5), 712–727. http://doi.org/10.1109/TMI.2007.895484

Bhateja, V., Singh, G., Srivastava, A., & Singh, J. (2014). Speckle reduction in ultrasound images using an improved conductance function based on Anisotropic Diffusion. *2014 International Conference on Computing for Sustainable Global Development (INDIACom)*, (March), 619–624. http://doi.org/10.1109/IndiaCom.2014.6828036

Chang, S. G., Yu, B., & Vetterli, M. (2000). Adaptive wavelet thresholding for image denoising and compression. *Image Processing, IEEE Transactions on*, *9*(9), 1532–1546.

Charbonnier, P., Blanc-Feraud, L., Aubert, G., & Barlaud, M. (1994). Two deterministic half-quadratic regularization algorithms for computed imaging. In *Image Processing,1994. IEEE International conference* (pp. 168–172).

Dong, J., Han, Z., Zhao, Y., Wang, W., Prochazka, A., & Chambers, J. (2017). Sparse Analysis Model Based Multiplicative Noise Removal with Enhanced Regularization. *Signal Processing*, *137*, 160–176. http://doi.org/10.1016/j.sigpro.2017.01.032

Donoho, D. L., & Johnstone, J. M. (1994). Ideal spatial adaptation by wavelet shrinkage. *Biometrika*. http://doi.org/10.1093/biomet/81.3.425

Dutt, V. (1995). Statistical analysis of ultrasound echo envelope. *Ultrasound Research Laboratory*, 181.

Guo, Z., Sun, J., Zhang, D., & Wu, B. (2012). Adaptive Perona – Malik Model Based on the Variable Exponent for Image Denoising. *Image Processing, IEEE Transactions on*, *21*(3), 958–967.

Hacini, M., Hachouf, F., & Djemal, K. (2014). A new speckle filtering method for ultrasound images based on a weighted multiplicative total variation. *Signal Processing*, *103*, 214–229. http://doi.org/10.1016/j.sigpro.2013.12.008

Hu, Z., & Tang, J. (2016). Cluster driven anisotropic diffusion for speckle reduction in ultrasound images. In *2016 IEEE International Conference on Image Processing (ICIP)* (pp. 2325–2329). IEEE. http://doi.org/10.1109/ICIP.2016.7532774

Kour, S., & Kaur, B. (2016). Hybrid filter with wavelet denoising and anisotropic diffusion filter for image despeckling. *2015 IEEE International Conference on Computer Graphics, Vision and Information Security, CGVIS 2015*, *115*(19), 17–21. http://doi.org/10.1109/CGVIS.2015.7449884

Kumar, R., & Rattan, M. (2012). Analysis Of Various Quality Metrics for Medical Image Processing. *International Journal of Advanced Research in Computer Science and Software Engineering*, *2*(11), 137–144.

Langtangen, H. P. (2013). Finite difference methods for diffusion processes, 1–21.

Liu, F., & Liu, J. (2012). Anisotropic diffusion for image denoising based on diffusion tensors. *Journal of Visual Communication and Image Representation*, *23*(3), 516–521. http://doi.org/10.1016/j.jvcir.2012.01.012

Liu, J., Huang, T., Xu, Z., & Lv, X. (2013). High-order total variation-based multiplicative noise removal with spatially adapted parameter selection. *Journal of the Optical Society of America A*, *30*(10), 1956. http://doi.org/10.1364/JOSAA.30.001956

ISSN: 2408-7920

Loizou, C. P., Pattichis, C. S., Christodoulou, C. I., Istepanian, R. S. H., Pantziaris, M., & Nicolaides, A. (2005). Comparative evaluation of despeckle filtering in ultrasound imaging of the carotid artery. *IEEE Transactions on Ultrasonics, Ferroelectrics, and Frequency Control*, *52*(10), 1653–1669. http://doi.org/10.1109/TUFFC.2005.1561621

Lv, X., Le, J., Huang, J., & Jun, L. (2013). A Fast High-Order Total Variation Minimization Method for Multiplicative Noise Removal. *Mathematical Problems in Engineering*, *2013*, 13. Retrieved from https://www.hindawi.com/journals/mpe/2013/834035/

Mahmoud, A. A., Rabaie, S. E. L., Taha, T. E., Zahran, O., & El-samie, F. E. A. (2013). Comparative Study of Different Denoising Filters for Speckle Noise Reduction in Ultrasonic B- Mode Images, (February), 1–8. http://doi.org/10.5815/ijigsp.2013.02.01

Maiseli, B. (2016). Diffusion-steered super-resolution method based on the Papoulis–Gerchberg algorithm. *IET Image Processing*, *10*(10), 683–692. http://doi.org/10.1049/iet-ipr.2015.0715

Maiseli, B. J., & Gao, H. (2016). Robust edge detector based on anisotropic diffusion-driven process. *Information Processing Letters*, *116*(5), 373–378. http://doi.org/10.1016/j.ipl.2015.12.003

Maleki, A., Narayan, M., & Baraniuk, R. G. (2013). Anisotropic nonlocal means denoising. *Applied and Computational Harmonic Analysis*, *35*(3), 452–482. http://doi.org/10.1016/j.acha.2012.11.003

Mastriani, M. (2008). New Wavelet-Based Superresolution Algorithm for Speckle Reduction in SAR Images, (1), 944–951.

Noe, S., Workshop, T., & Palmas, L. (2006). DIFFUSION FILTERS IN IMAGE PROCESSING : A BRIEF REVIEW Burak Acar. *Similar NoE TensorWorkshop, Las Palmas*, (November).

Perona, P., & Malik, J. (1990). Scale-space and edge detection using anisotropic diffusion. *IEEE Transactions on Pattern Analysis and Machine Intelligence*, *12*(12), 629–639. http://doi.org/10.1109/34.56205

Ramos-Llordén, G., Vegas-Sánchez-Ferrero, G., Martin-Fernandez, M., Alberola-López, C., & Aja-Fernández, S. (2015). Anisotropic diffusion filter with memory based on speckle statistics for ultrasound images. *IEEE Transactions on Image Processing*, *24*(1), 345–358. http://doi.org/10.1109/TIP.2014.2371244

Rudin, L. I., Osher, S., & Fatemi, E. (1992). Nonlinear total variation based noise removal algorithm. *Physica D*, *60*(1–4), 259–268. http://doi.org/doi:10.1016/0167-2789(92)90242-F

Shama, M. G., Huang, T. Z., Liu, J., & Wang, S. (2016). A convex total generalized variation regularized model for multiplicative noise and blur removal. *Applied Mathematics and Computation*, *276*(March), 109–121. http://doi.org/10.1016/j.amc.2015.12.005

Wang, Z., & Bovik, A. C. (2009). Mean squared error: Lot it or leave it? A new look at signal fidelity measures. *IEEE Signal Processing Magazine*, *26*(1), 98–117. http://doi.org/10.1109/MSP.2008.930649

Wang, Z., Bovik, A. C., Sheikh, H. R., & Simoncelli, E. P. (2004). Image quality assessment: From error visibility to structural similarity. *IEEE Transactions on Image Processing*, *13*(4), 600–612. http://doi.org/10.1109/TIP.2003.819861

Weickert, J., & Benhamouda, B. (1997). A semidiscrete nonlinear scalespace theory and its relation to the Perona–Malik paradox. In *Advances in computer vision* (pp. 1–10).

ISSN: 2408-7920

Wu, B., Ogada, E. A., Sun, J., & Guo, Z. (2014). A Total Variation Model Based on the Strictly Convex Modification for Image Denoising. *Abstract and Applied Analysis*, *2014*, 16. http://doi.org/948392

Wu, Y., & Feng, X. (2015). Speckle Noise Reduction via Nonconvex High Total Variation Approach. *Mathematical Problems in Engineering*, *2015*, 11.

Xu, J., Jia, Y., Shi, Z., & Pang, K. (2016). An improved anisotropic diffusion filter with semi-adaptive threshold for edge preservation. *Signal Processing*, *119*, 80–91. http://doi.org/10.1016/j.sigpro.2015.07.017

Zhang, J., Lin, G., Wu, L., Wang, C., & Cheng, Y. (2015). Wavelet and fast bilateral filter based de-speckling method for medical ultrasound images. *Biomedical Signal Processing and Control*, *18*, 1–10. http://doi.org/10.1016/j.bspc.2014.11.010

ISSN: 2408-7920